Geophysical Journal International

Geophys. J. Int. (2012) **191,** 64–77 doi: 10.1111/j.1365-246X.2012.05622.x

Hysteresis and thermomagnetic properties of particle-sized fractions from loess and palaeosol samples spanning 22 Myr of accumulation on the Chinese Loess Plateau

Qingzhen Hao,[1,2] Frank Oldfield,[2] Jan Bloemendal[2] and Zhengtang Guo[1]

[1] *Key Laboratory of Cenozoic Geology and Environment, Institute of Geology and Geophysics, Chinese Academy of Sciences, Beijing* 100029, *China*
[2] *School of Environmental Sciences, University of Liverpool, Liverpool,* L69 7ZT, *UK. E-mail: oldfield.f@gmail.com*

Accepted 2012 July 20. Received 2012 July 20; in original form 2012 April 25

SUMMARY

Hysteresis loop measurements and thermomagnetic experiments were carried out to characterize magnetic mineralogy and magnetic grain size in a suite of particle-size fractioned samples from the Chinese Loess Plateau, representing the main changes in magnetic properties over the last 22 Myr. We find that (1) the ferrimagnets in the detrital fractions (>8 μm) younger than 14 Ma show a magnetite-type Curie temperature, whereas those older than 15 Ma have a Curie temperature slightly over 600 °C owing to low-temperature oxidation. (2) The dominant ferrimagnets in the clay fractions (<2 μm) are most likely to be maghemite. (3) Both the hysteresis plots and thermomagnetic experiments reinforce previous indications from low-temperature experiments that paramagnetic minerals make a major contribution to the clay fractions in all the samples considered. (4) The degree of oxidation indicated by the thermomagnetic curves is highest in the clays and next highest in the oldest coarse fractions. (5) Day plots provide limited and potentially misleading information on the differences between fine-grained pedogenic and coarse-grained detrital ferrimagnetic assemblages, even when allowance is made for the effects of hematite on the quotients used. This study reinforces the view that measurements on bulk samples alone obscure critical distinctions between pedogenic and detrital components.

Key words: Environmental magnetism; Magnetic and electrical properties; Asia.

1 INTRODUCTION

The Chinese Loess Plateau (CLP) holds what is probably the most detailed and continuous terrestrial archive of Neogene and Quaternary environmental change anywhere on the planet. Unlocking the significance of this record rests in the first instance on the analysis and evaluation of some of the key properties of potential value in palaeoenvironmental reconstruction. Among these properties, those derived from rock magnetic measurements have often been used, especially as indicators of Quaternary palaeoclimates (e.g. Heller & Evans 1995; Liu *et al.* 1995; Maher & Thompson 1999; Evans & Heller 2001; Hao & Guo 2005).

In the wake of the paper by Guo *et al.* (2002) confirming the eolian origin and age of the key QA–I Miocene section near Qinan, in the western part of the CLP, several publications have been devoted to the rock magnetic properties of this and other overlapping sections that together span the whole of the last 22 Myr. These papers have detailed (i) the routine magnetic properties of a sequence of bulk loess and palaeosol samples representative of each of the main stages of accumulation (Hao *et al.* 2008a), (ii) particle size based measurements that separately characterize the pedogenic and detrital components of the samples (Hao *et al.* 2008b; Oldfield *et al.* 2009) and (iii) the evidence, from magnetic measurements and diffuse reflectance spectroscopy (DRS), for changing hematite and goethite concentrations in both bulk and particle-sized samples (Hao *et al.* 2009). In addition, geochemical and grain size analyses have also been reported (Qiao *et al.* 2006; Liang *et al.* 2009).

In this paper, our main aim is to present and evaluate evidence from hysteresis loop measurements and thermomagnetic experiments. Most of the previous studies using this approach have based measurements on bulk samples (e.g. Liu *et al.* 1992; Fukuma & Torii 1998; Deng *et al.* 2004; Wang *et al.* 2006), in some cases using CBD extraction to remove the fine pedogenic grains (Deng *et al.* 2005). Since the studies by Zheng *et al.* (1991) and Chen *et al.* (1995), it has been clear that bulk sample measurements obscure the complex nature of loess and palaeosol magnetic mineralogy, especially in samples where both pedogenic and detrital minerals are present. Several recent studies recognize this and take a more sophisticated approach by basing hysteresis measurements and thermomagnetic experiments on particle size fractions (Spassov *et al.* 2003) or combining particle separation with magnetic extraction (Liu *et al.* 2003). All these studies are restricted to sections of Quaternary age. This study is the first to apply these techniques to samples spanning the last 22 Myr. Although a rather robust framework has emerged for interpreting the rock-magnetic properties of the Quaternary sequences on the CLP, this is not yet the case for

© 2012 The Authors
Geophysical Journal International © 2012 RAS

the longer term record from early Miocene times onwards. In this paper, we aim to advance this aspect of loess-based research since it is an essential precursor for developing secure palaeoenvironmental inferences from the rock-magnetic record.

Figs 2 and 3 set our new results (Figs 4–8 and Tables 1–3) in the context created by our previous research. They establish the overall sequence of rock-magnetic changes already documented and identify the levels from which clay and coarse fraction subsamples of palaeosol and loess used in this paper have been obtained. 22 of the total of 26 levels sampled predate the onset of the Quaternary period. Thus, this paper presents the first analysis of the hysteresis and thermomagnetic properties of the pedogenic and detrital fractions of eolian sediments and palaeosols spanning virtually the whole of the Neogene.

2 SITES AND SAMPLES

The samples come from three sites: Xifeng (XF, 0–3.4 Ma), Dongwan (DW, 3.5–7 Ma) and Qinan (QA–I, 6.2–22 Ma; Fig. 1). The QA–I and DW sections are recently discovered Neogene loess–palaeosol sequences (Guo *et al.* 2002; Hao & Guo 2004). Since there are no well-preserved loess sections postdating 3.6 Ma from the western CLP close to the DW and QA–I sections, samples dating from post 3.6 Ma come from the well-documented XF section, 210 km to the east (Sun *et al.* 1998; Guo *et al.* 1998, 2001). Our samples were chosen from the set of 106 used to characterize the changing magnetic properties of the loess and intervening palaeosols over the whole period (Hao *et al.* 2008a). Fig. 2 shows selected bulk magnetic properties for the full sample set and provides part of the context for this study (Hao *et al.* 2008a; Oldfield *et al.* 2009). Fig. 3 shows selected results from routine magnetic measurements on the <2 μm (Fig. 3a) and >8 μm (Fig. 3b) fractions for all the particle-sized samples. The samples used in this study are separately identified in Fig. 3. They have been chosen to represent the main zones noted in Fig. 2 and, in most cases, they have been taken from loess/palaeosol couplets.

3 METHODS

3.1 Particle size separation

Bulk samples were separated by the pipette method into four grain size fractions: <2, 2–4, 4–8 and >8 μm using the methods outlined in Hao *et al.* (2008b). The pipetted subsamples were freeze-dried to avoid any oxidation of iron minerals. The low contribution of material >63 μm in all but the youngest Pleistocene loess rendered it unnecessary for present purposes to sieve the samples before pipette analysis. Our previous research demonstrates that the <2 and >8 μm fractions can be used to represent the pedogenic and detrital fractions, respectively, and these two fractions account for 73.5–90.6 per cent (80.1 ± 4.2 per cent, $n = 26$) of the bulk samples (Hao *et al.* 2008b).

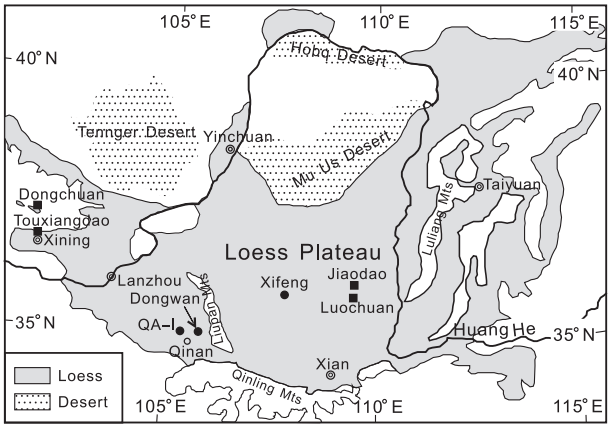

Figure 1. Location map showing the Loess Plateau and the sites mentioned. Solid circles indicate the sites in this study and solid squares, the sites in cited references.

3.2 Hysteresis experiments

Hysteresis measurements of clay (<2 μm) and coarse (>8 μm) fractions separated from 16 bulk loess and palaeosol samples were performed using a Micromag VSM 3900 with a maximum field of 1.5 T at the Geomagnetism and Geochronology Laboratory, Institute of Geology and Geophysics, Chinese Academy of Sciences (IGGCAS). Subsequently, the IRM at 1.5 T was demagnetized in a stepwise sequence of backfields to obtain remanent coercivity (B_{cr}) values. Saturation magnetization (M_s) and coercivity (B_c) were calculated after subtracting the paramagnetic contribution identified by the slope above 1.05 T (70 per cent of maximum field). Paramagnetic susceptibility (χ_{para}) was calculated by the linear-fitted portion between 1.05 and 1.5 T. The ferrimagnetic susceptibility (χ_{ferri}) is calculated as $\chi_{ferri} = -\chi_{para}$, where χ is low-field magnetic susceptibility.

3.3 Thermomagnetic experiments

The thermomagnetic experiments were conducted on the same 32 fractionized samples using a VFTB with a maximum field of 0.75 T at the Geomagnetism Laboratory, University of Liverpool. The samples were heated in air from ∼60 to 700 °C, then cooled to ∼80 °C in an applied field of 0.75 T. To investigate magnetic mineral alternation at lower temperature intervals, parallel subsamples of clay and coarse fractions from two soil/loess couplets of early Pleistocene and early Miocene were used in thermomagnetic measurements with different maximum temperatures up to 350 °C. New subsamples (non-heated) were used in each new run. These measurements were conducted, at a heating and cooling rate of 40 °C min^{-1}, on a VFTB instrument at the Geomagnetism and Geochronology Laboratory of IGGCAS.

3.4 Viscous loss of IRM measurements

Clay and coarse fractions from six samples were selected for measuring viscous loss of IRM. In the case of the clay fractions, IRM was acquired at 20, 40, 100 and 800 mT using an MMPM5 Pulse Magnetizer. After each step, IRM was measured continuously in zero field for over 1000 s using a Molspin spinner magnetometer with a noise level 0.1×10^{-8} Am^2. In the case of the coarse fractions, the same procedure was used, but only for two fields, 100 and 800 mT.

3.5 Susceptibility and remanence measurement

Low-frequency magnetic susceptibility (χ), frequency dependent magnetic susceptibility (χ_{fd}), susceptibility of anhysteretic remanent magnetization (χ_{ARM}), isothermal remanent magnetization (IRM) and saturation IRM (SIRM) were determined by routine

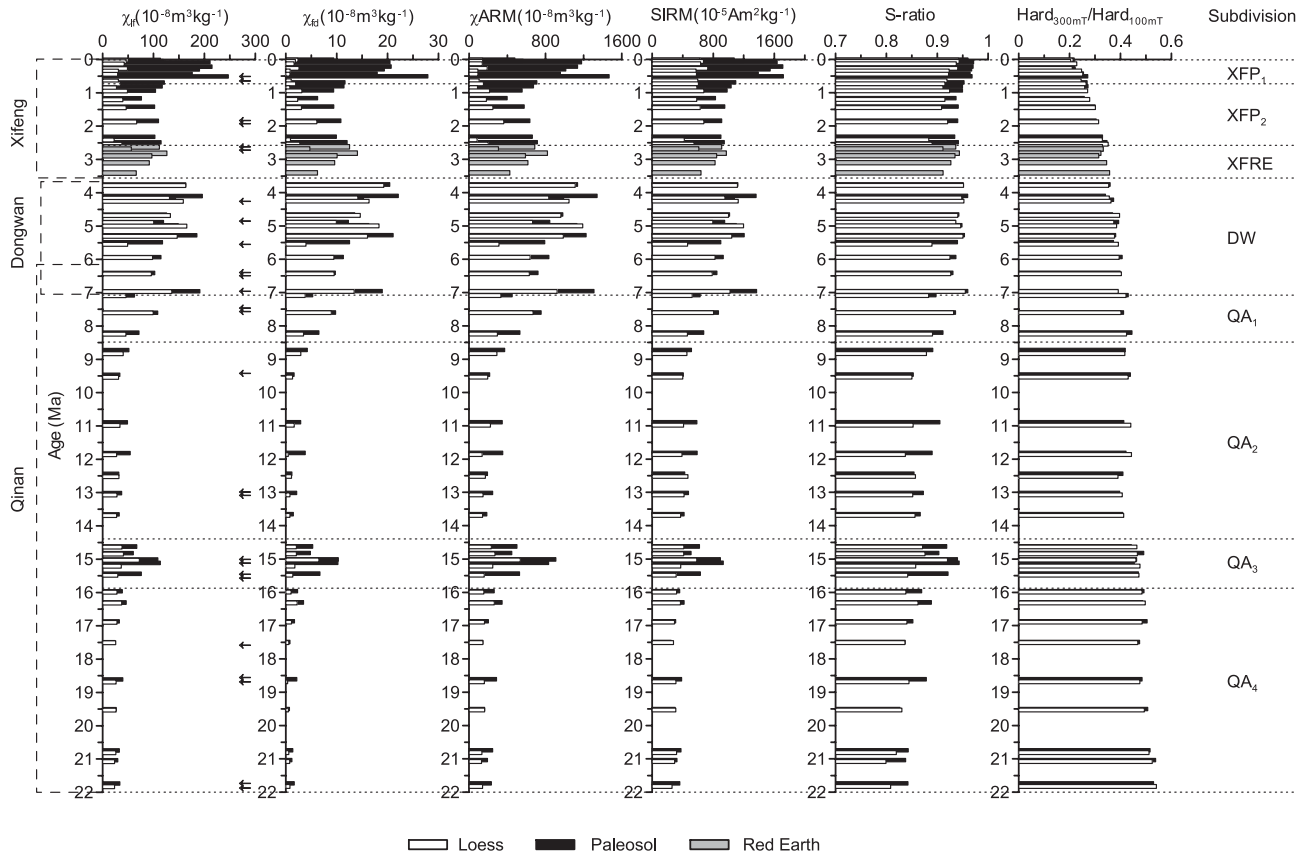

Figure 2. Routine magnetic properties and the quotients derived from them for the selected samples of eolian deposits from the Chinese Loess Plateau spanning the last 22 Myr. All the results are calculated on a carbonate-free basis. The eight sample groups shown on the right-hand side are defined by routine magnetic properties (Hao *et al.* 2008a). The arrows in the left-hand graph identify the samples particle-sized by pipette analysis.

methods as described in Hao *et al.* (2008a). *S*-ratio is calculated as $S = 0.5 \times [(-\mathrm{IRM}_{-0.3\mathrm{T}}/\mathrm{SIRM}) + 1]$ (Bloemendal *et al.* 1992).

4 RESULTS

Fig. 4 shows the hysteresis loops corrected for paramagnetism for all the clay fractions and coarse fractions. Table 1(a and b) records the main properties derived from the hysteresis loop measurements for the clays and coarse fractions, respectively. Several parameters derived from previous measurements and from DRS experiments (Hao *et al.* 2008b, 2009) have been added for comparison.

Fig. 5(a) shows the magnetization versus temperature curves for representative clay and coarse fractions. Superimposed on the heating and cooling curves that include the paramagnetic effect, are heating curves (in red) from which the paramagnetic effect has been subtracted. Fig. 5(b) shows the results of measurements of magnetization versus temperature with different maximum temperatures up to 350 °C for representative clay and coarse fractions, respectively. Table 2 compares the magnetic properties of selected clay (<2 μm) and coarse (>8 μm) fractions and their 220, 300 °C thermal products, respectively.

Table 3 gives the loss IRM of from 100 to 1000 s at each step in IRM acquisition as a percentage of the IRM at 100 s. On an average, viscous loss at 20 mT in the clay fractions exceeds that in the coarse fractions by a factor of 4.5. Most of the loss in the fine fractions is in the low-coercivity components.

From the above figures and tables, we make the following initial observations.

4.1 Hysteresis loops

(1) 'Wasp-waisted' loops are more marked and more frequent in the clay than in the coarse fraction. They are especially notable in the clay fraction of the most recent loess sample, from 0.64 Ma and in most samples older than 13 Ma.

(2) Paramagnetic susceptibility (χ_{para}) in the clay fractions is relatively high, varying between 13.41 and 16.28 $\times$ 10^{-8} $\mathrm{m^3\,kg^{-1}}$ (Table 1). Comparison between loess and palaeosol values in couplets shows generally higher values in the palaeosols, it is quite independent of ferrimagnetic susceptibility (χ_{ferri}) which varies by over two orders of magnitude, with the oldest sample the weakest and the youngest the strongest. As a percentage of total susceptibility, χ_{para} ranges from 3.77 per cent in the youngest sample to 55.23 per cent in the oldest, with consistently high percentages in samples older than 13 Ma, except for the soil sample (99QW–1603) from the high susceptibility interval, 14.4–15.9 Ma.

(3) The clay samples with the highest χ_{para} percentages also have the lowest χ'_{fd} per cent values. Most are also marked by lower S-ratio values and relatively 'harder' DC demagnetization of IRM values in the routine measurements.

(4) Paramagnetic susceptibility in the coarse fractions is lower than in the clays and varies between 3.52 and 6.37 $\times$ 10^{-8} $\mathrm{m^3\,kg^{-1}}$ (Table 1). Comparison between loess and palaeosol values in couplets shows generally higher values in the loess, and the highest values for χ_{para} as a percentage of total susceptibility are also in loess layers. However, in contrast to the clays, there is no apparent trend through time.

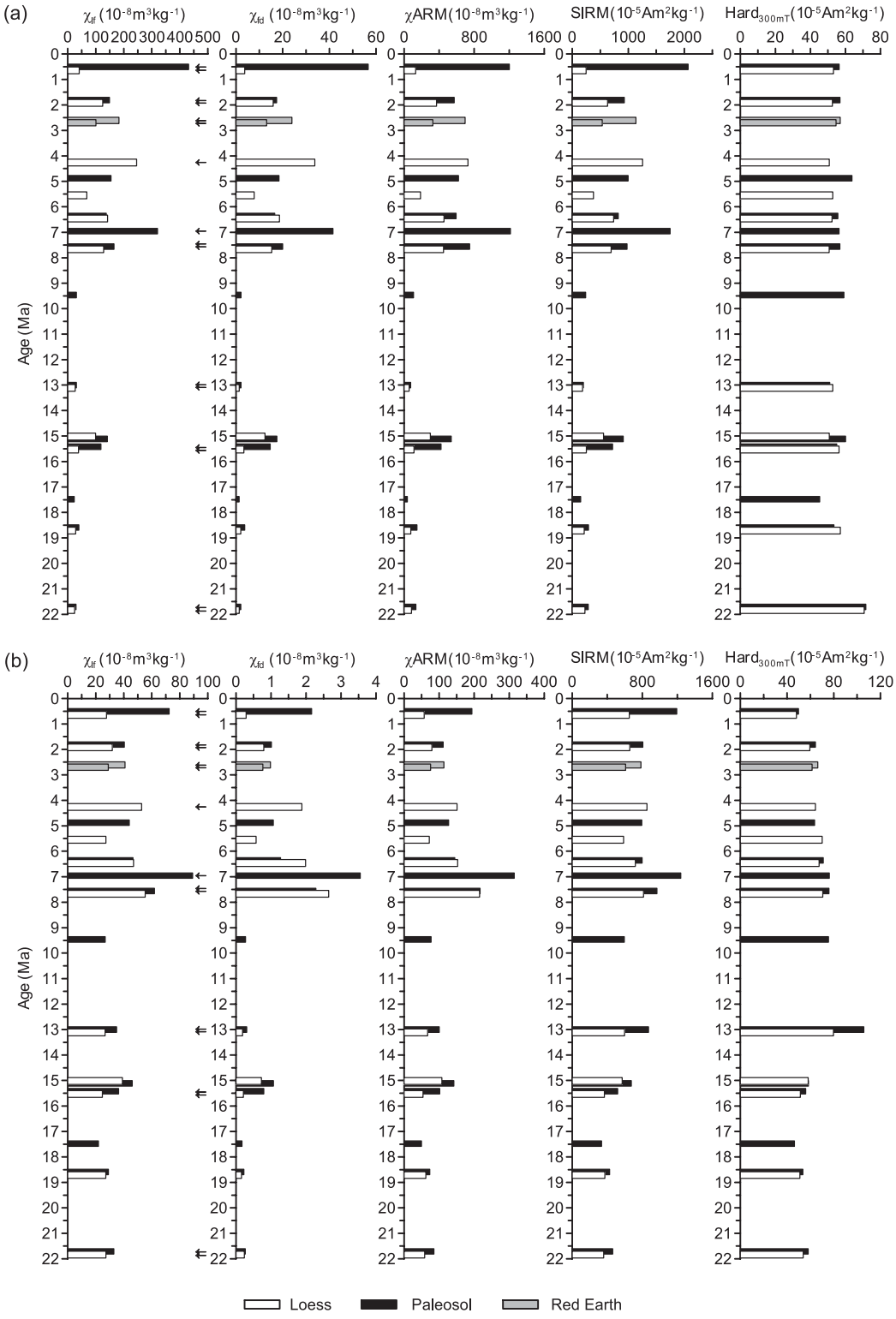

Figure 3. Selected results of routine magnetic measurements on the <2 μm (a) and >8 μm (b) fractions for all the particle-sized samples. The arrows in the left-hand graph identify the samples used in this study.

(5) χ_{ferri} in the coarse fraction varies only by a factor of ∼4 and is consistently higher in palaeosol layers.

(6) Values of M_s (8.07–157.13 × 10^{-3} $Am^2\,kg^{-1}$) and M_{rs} (2.03–24.02 × 10^{-3} $Am^2\,kg^{-1}$) are more variable in the clays than in the coarse fractions (21.76–72.49 × 10^{-3} $Am^2\,kg^{-1}$ for M_s and 3.48–13.81 × 10^{-3} $Am^2\,kg^{-1}$ for M_{rs}), with maxima in the Pleistocene and late Miocene palaeosols, and minima in the older loess layers. B_c values, except in the three of six of the oldest samples, are sample by sample lower in the clay than in the coarse fractions, and, except in four of six oldest samples B_{cr} values also are lower in the clays than in the corresponding coarse fractions.

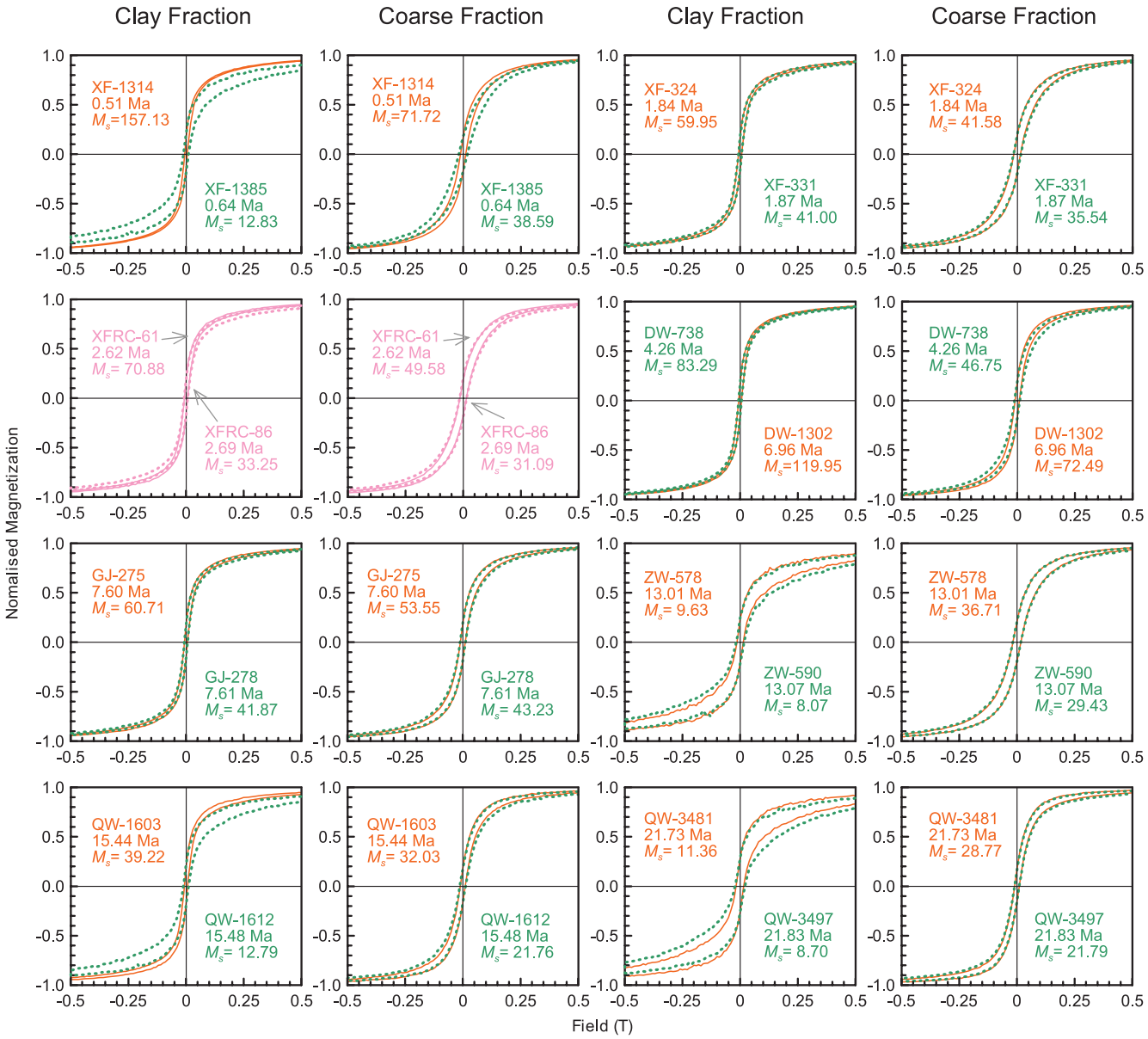

Figure 4. The hysteresis loops corrected for paramagnetism for all the clay (<2 μm) and coarse (>8 μm) fractions over the last 22 Myr. The orange solid lines refer to particle separates from palaeosol samples and the green dot lines, those from loess samples. M_s ($\times 10^{-3}$ Am^2 kg^{-1}) for each sample is also given. In the case of the 'Red Earth' samples from Xifeng (in pink) it is not possible to distinguish loess and palaeosol parts of the section. For the clay fractions, all the hysteresis loops are closed in fields below 1 T. For the coarse fractions, they are closed in fields below 0.5 T, except for the two earliest samples in which the loops close at around 0.6 T.

(7) Although, in each couplet, χ_{fd} values are consistently higher in soil than in loess and χ_{fd} values in samples postdating 8 Ma are generally between one and two orders of magnitude higher than in the Miocene samples with lowest χ values, χ_{fd} expressed as a percentage of χ_{ferri} do not vary significantly either between soil and palaeosol samples, or with age.

4.2 Thermomagnetic experiments

(1) The uncorrected heating curves for the clay fractions are generally concave downwards; in some cases, the concavity is present throughout, in others, it is most clearly marked above 150 °C.

(2) The heating curves for the coarse fractions are generally convex upwards though the form of the convexity varies. In samples younger than 7 Ma, the main convexity is in the temperature range 450–580 °C. In older samples, this feature is less clearly marked. In many samples, including those older than 7 Ma, there is an inflexion in the heating curve between 200 and 300 °C.

(3) In the case of the clay fractions, there is no clear indication of a magnetite-type Curie temperature (T_c) at 585 °C. The curves from which the paramagnetic effect has been subtracted generally point to a T_c just above 600 °C.

(4) In the case of the coarse fractions younger than ∼14 Ma, a magnetite-type T_c at ∼585 °C is clearly indicated in both the uncorrected and corrected heating curves. In older samples, the evidence for a definable T_c is more difficult to discern and there are indications in the corrected curves that the oldest samples have a higher T_c.

© 2012 The Authors, *GJI*, **191**, 64–77
Geophysical Journal International © 2012 RAS

Table 1. Hysteresis properties plotted alongside selected rock magnetic properties and hematite content for the clay (<2 μm) (a) and coarse (>8 μm) (b) fractions over the last 22 Myr.

Age	Sample	Lithology	Percentage	χ	χ_{fd}	χ_{para}	χ_{ferri}	M_{rs}	M_s	B_{cr}	B_c	M_{rs}/M_s	B_{cr}/B_c	χ_{para}/χ	χ'_{fd} (per cent)	χ_{para}/M_s	*S*-ratio	$Hard_{100mT}$ per cent	Hm	$HIRM_{1.5T,AF}$	$Hard_{100mT}$
(Ma)			(mass per cent)	($10^{-8}m^3\,kg^{-1}$)				($10^{-3}Am^2\,kg^{-1}$)		(mT)				(per cent)		($10^{-5}mA^{-1}$)			($g\,kg^{-1}$)	($10^{-5}Am^2\,kg^{-1}$)	
0.51	XF-1314	S5SS1	24.86	431.42	56.67	16.27	415.15	24.02	157.13	14.85	5.92	0.15	2.51	3.77	13.65	0.10	0.97	5.55	27.11	75.56	114.77
0.64	XF-1385	L6	12.04	41.04	3.74	16.06	24.98	2.70	12.83	43.29	11.24	0.21	3.85	39.13	14.98	1.25	0.78	38.58	19.52	62.94	94.85
1.84	XF-324	S25	19.45	148.65	17.39	16.28	132.37	10.45	59.95	18.30	7.59	0.17	2.41	10.95	13.14	0.27	0.94	11.55	16.41	67.46	107.28
1.87	XF-331	L26	21.36	124.87	15.93	15.93	108.94	7.13	41.00	18.28	7.07	0.17	2.59	12.76	14.62	0.39	0.92	15.42	15.90	61.42	97.07
2.62	XFRC-61	Red Earth	25.77	183.15	23.98	15.89	167.26	13.13	70.88	16.50	7.27	0.19	2.27	8.68	14.34	0.22	0.95	9.65	14.83	66.87	109.73
2.69	XFRC-86	Red Earth	20.51	100.66	13.09	15.04	85.62	6.26	33.25	19.39	7.75	0.19	2.50	14.94	15.29	0.45	0.90	17.93	13.05	60.47	96.32
4.26	DW-738	Loess	35.85	246.04	33.80	14.97	231.07	14.12	83.29	15.32	6.43	0.17	2.38	6.08	14.63	0.18	0.96	8.70	21.63	69.15	109.16
6.96	DW-1302	Soil	35.24	320.62	41.51	15.95	304.67	20.63	119.95	14.84	6.34	0.17	2.34	4.98	13.63	0.13	0.97	6.02	23.73	65.97	105.16
7.60	GJ-275	Soil	36.56	165.04	20.00	15.17	149.88	10.54	60.71	16.82	6.84	0.17	2.46	9.19	13.34	0.25	0.94	10.54	20.36	62.93	102.97
7.61	GJ-278	Loess	34.05	128.10	15.32	14.77	113.33	7.39	41.87	18.10	6.97	0.18	2.60	11.53	13.52	0.35	0.93	13.52	19.13	61.04	93.86
13.01	ZW-578	Soil	37.85	31.05	2.13	14.97	16.08	2.34	9.63	58.47	13.58	0.24	4.31	48.22	13.26	1.55	0.74	44.33	13.56	60.55	87.38
13.07	ZW-590	Loess	30.90	26.17	1.40	14.43	11.74	2.03	8.07	93.50	17.39	0.25	5.38	55.14	11.96	1.79	0.71	47.05	16.38	60.02	86.33
15.44	QW-1603	Soil	38.75	118.40	14.66	14.33	104.07	7.51	39.22	17.57	7.17	0.19	2.45	12.10	14.09	0.37	0.92	13.55	21.37	62.30	97.49
15.48	QW-1612	Loess	29.64	38.81	3.37	14.75	24.07	2.79	12.79	39.20	11.37	0.22	3.45	37.99	14.02	1.15	0.78	38.66	20.61	61.25	96.94
21.73	QW-3481	Soil	42.91	29.51	2.09	13.80	15.71	3.27	11.36	58.03	16.39	0.29	3.54	46.77	13.28	1.21	0.75	43.30	22.75	81.29	123.59
21.83	QW-3497	Loess	37.48	24.28	1.38	13.41	10.87	2.56	8.70	124.15	21.77	0.29	5.70	55.23	12.72	1.54	0.69	54.05	22.82	79.14	122.37
(b)																					
0.51	XF-1314	S5SS1	58.53	72.38	2.16	4.48	67.90	12.49	71.72	31.41	11.37	0.17	2.76	6.19	3.18	0.06	0.96	20.75	2.96	78.11	247.68
0.64	XF-1385	L6	78.55	27.65	0.29	5.67	21.98	6.83	38.59	56.29	18.50	0.18	3.04	20.52	1.32	0.15	0.93	31.56	1.20	70.63	205.88
1.84	XF-324	S25	63.60	40.37	1.01	5.08	35.29	7.89	41.58	44.09	14.45	0.19	3.05	12.58	2.86	0.12	0.92	29.31	2.44	85.89	236.26
1.87	XF-331	L26	63.97	31.85	0.79	5.62	26.24	7.11	35.54	50.08	15.97	0.20	3.14	17.63	3.02	0.16	0.91	30.93	2.52	83.66	203.03
2.62	XFRC-61	Red Earth	58.10	40.90	0.98	4.94	35.96	8.77	49.58	43.43	14.20	0.18	3.06	12.07	2.74	0.10	0.92	29.12	2.41	95.11	228.38
2.69	RC-86	Red Earth	64.83	28.92	0.77	5.79	23.14	6.27	31.09	41.27	15.00	0.20	2.75	20.00	3.32	0.19	0.90	33.03	2.19	81.04	201.31
4.26	DW-738	Loess	42.42	52.76	1.88	4.73	48.03	8.77	46.75	32.35	11.50	0.19	2.81	8.96	3.91	0.10	0.92	24.79	3.34	86.26	211.74
6.96	DW-1302	Soil	39.02	89.11	3.55	5.13	83.98	13.81	72.49	23.23	9.43	0.19	2.46	5.76	4.23	0.07	0.94	18.38	4.19	106.03	227.76
7.60	GJ-275	Soil	37.35	61.85	2.28	5.41	56.44	10.21	53.55	29.30	10.82	0.19	2.71	8.74	4.04	0.10	0.92	24.16	3.76	96.32	233.78
7.61	GJ-278	Loess	40.49	55.26	2.65	6.37	48.90	8.30	43.23	33.40	11.57	0.19	2.89	11.52	5.41	0.15	0.91	26.36	4.46	95.48	214.66
13.01	ZW-578	Soil	41.04	34.82	0.30	4.63	30.19	7.43	36.71	57.24	17.25	0.20	3.32	13.28	1.00	0.13	0.88	37.52	1.30	128.63	326.95
13.07	ZW-590	Loess	51.34	26.65	0.19	5.23	21.42	6.06	29.43	64.84	17.20	0.21	3.77	19.63	0.86	0.18	0.87	39.19	1.45	108.78	234.17
15.44	QW-1603	Soil	39.21	36.24	0.79	4.81	31.43	5.75	32.03	35.08	10.96	0.18	3.20	13.28	2.53	0.15	0.89	26.75	2.52	75.69	138.77
15.48	QW-1612	Loess	53.43	24.67	0.21	4.95	19.72	3.83	21.76	50.94	12.49	0.18	4.08	20.06	1.07	0.23	0.86	35.66	1.87	73.46	130.88
21.73	QW-3481	Soil	39.61	32.96	0.26	3.52	29.44	4.75	28.77	38.98	10.42	0.16	3.74	10.69	0.90	0.12	0.87	28.55	3.46	77.02	131.95
21.83	QW-3497	Loess	44.29	27.19	0.24	4.17	23.02	3.48	21.79	43.86	10.14	0.16	4.33	15.33	1.03	0.19	0.85	32.31	3.67	68.75	115.93

Notes: Percentage refers to content of the <2 μm in (a) and >8 μm in (b) fraction determined by pipette method; χ, low-field susceptibility; χ_{fd}, frequency-dependent susceptibility; χ_{para}, paramagnetic susceptibility; χ_{ferri}, ferrimagnetic susceptibility; M_{rs}, saturation remanence; M_s, saturation magnetization; B_{cr}, coercivity of remanence; B_c, coercivity; χ'_{fd} per cent, $\chi_{fd}/\chi_{ferri} \times 100$ per cent; *S*-ratio, $0.5 \times [(-IRM_{-0.3T}/SIRM) + 1]$; $Hard_{100mT}$, $0.5 \times (IRM_{-0.1T} + SIRM_{1T})$; $Hard_{100mT}$ per cent, $Hard_{100mT}/SIRM_{1T} \times 100$ per cent; Hm, hematite content determined by DRS method; $HIRM_{1.5T,AF}$, the residual IRM imparted in a DC field of 1.5 T after the AF demagnetization with a peak field of 200 mT.

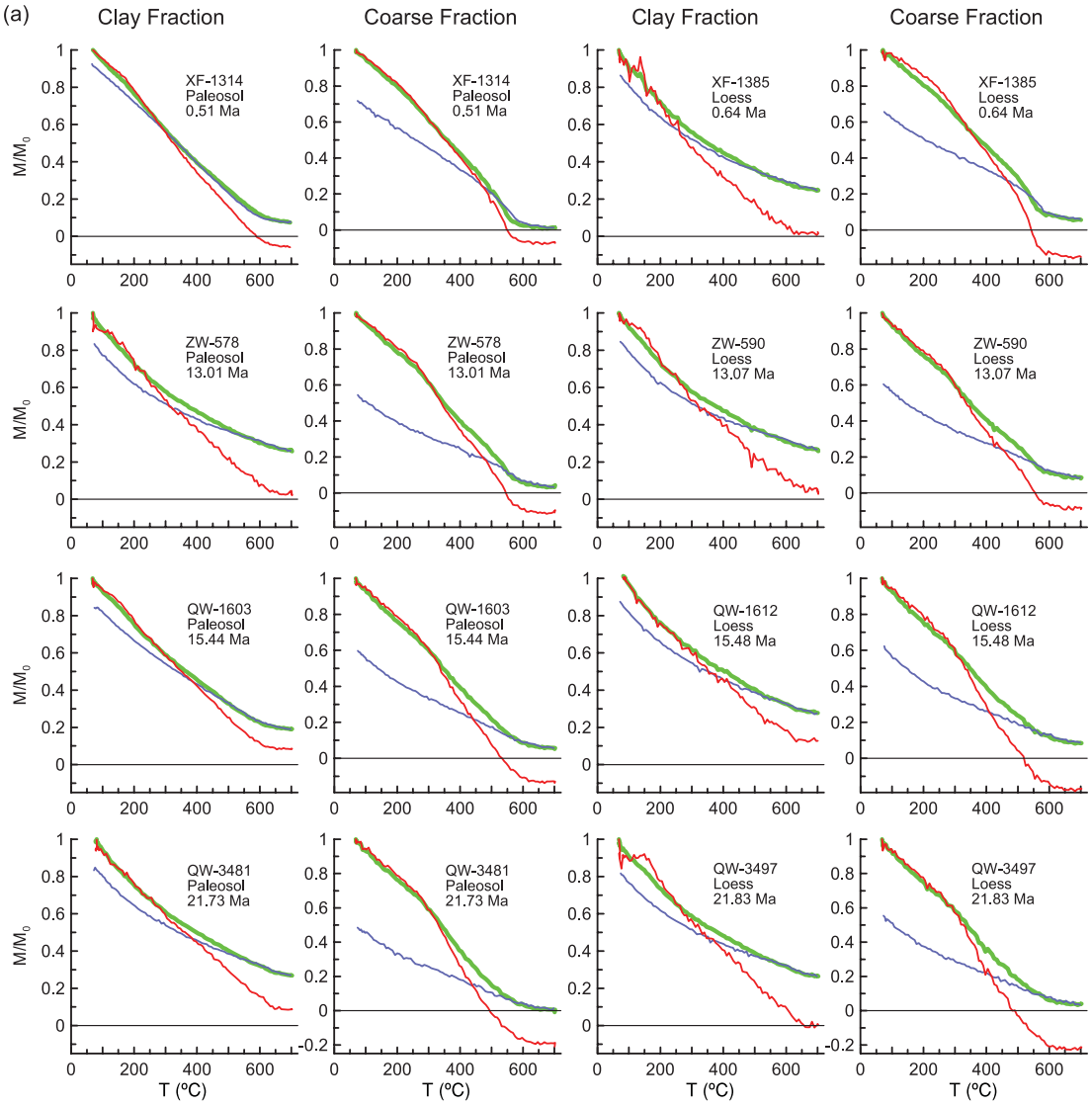

Figure 5. Thermomagnetic curves (a) for the representive clay (<2 μm) and coarse (>8 μm) fractions over the last 22 Myr, and partial thermomagnetic curves (b) for selected clay (<2 μm) and coarse (>8 μm) fractions. The clay and coarse fractions of palaeosols and loess between 0.64 and 8 Ma have similar thermomagnetic curves to those of the youngest palaeosol sample XF-1314 and loess sample XF-1385, respectively, and are not shown. The inserted diagrams in b show the results of a second heating run on the same subsamples, up to 250 °C. The green, red and blue lines indicate the uncorrected heating curves, corrected heating curves from which the paramagnetic contribution is subtracted and cooling curves, respectively. The possible alteration of paramagnetic minerals during heating is not considered.

(5) In the clay fractions, the uncorrected heating curve never falls to zero and at 700 °C the remaining normalized magnetization always exceeds that in the coarse fraction at the same temperature.

(6) In both clay and coarse fractions, magnetization at the end of the cooling sequence is always lower than at the beginning of the experiment.

(7) In the coarse fractions, although the main inflexion in the heating curve is close to the T_c of magnetite (i.e. ∼585 °C), the main inflexion in the cooling curve, where detectable, occurs at a slightly higher temperature. This is most clearly seen in the most recent samples and becomes virtually undetectable in samples older than 13 Ma.

(8) In the corrected heating curves, magnetization at high temperatures mostly plots below the zero line. This is much more extreme and consistent in the case of the coarse fractions than in the fine fractions.

(9) In the partial thermomagnetic experiments on clay samples (Fig. 5b), there is slight divergences around 150–200 °C between the heating and cooling trajectories. By contrast, in the coarse fractions, the final value lies below the initial value once heating proceeds above ∼300 °C.

5 DISCUSSION

Here, we focus on those aspects of the data that enhance or challenge the inferences derived from the previously published studies. In this regard, two aspects of the data are of special interest: the additional insights into the mineralogy of the ferrimagnetic minerals present provided by the thermomagnetic experiments, and the separation of the susceptibility record into ferrimagnetic and paramagnetic components.

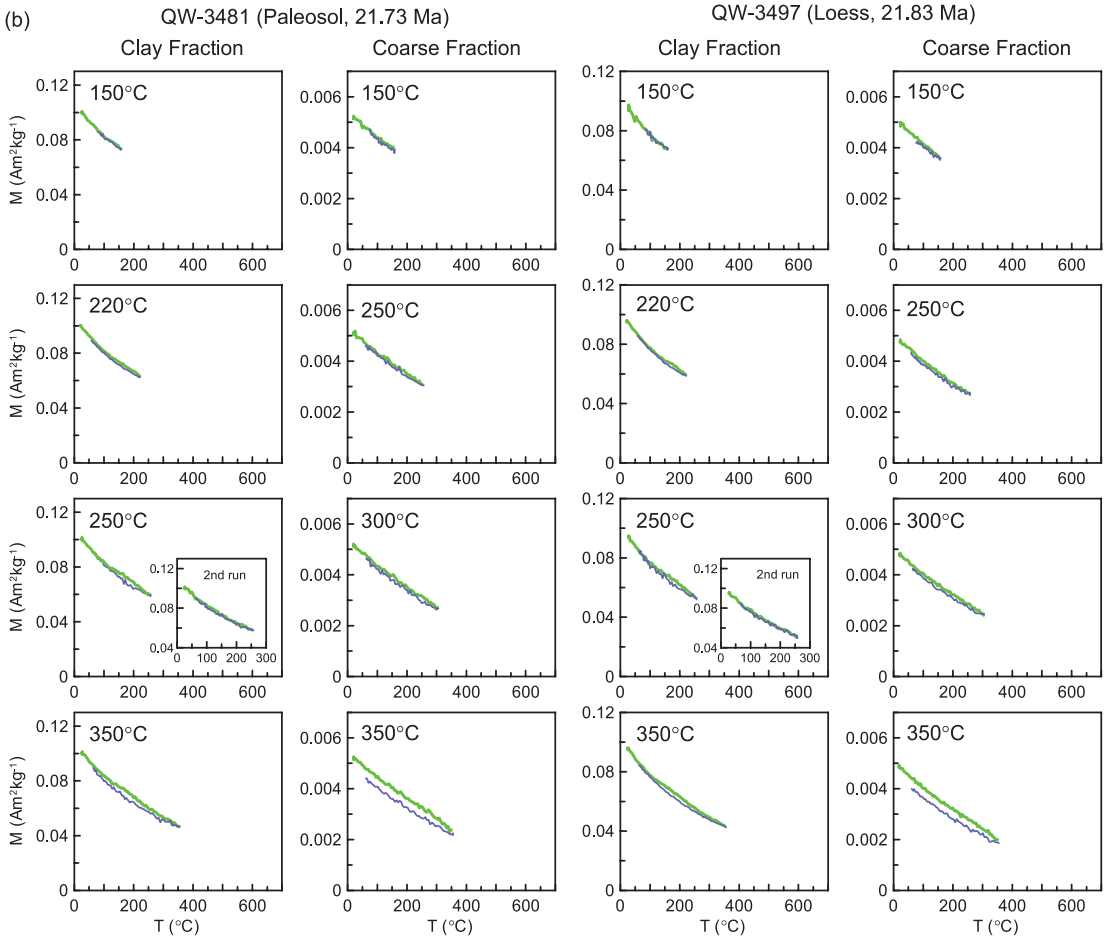

Figure 5. (*Continued.*)

5.1 Magnetic mineralogy of the clay fractions

In the clay fractions, one of the most distinctive features of both the hysteresis loops and the thermomagnetic experiments is the evidence for varying, in some cases, strong contributions from paramagnetic minerals. Where the hysteresis-based calculations indicate that paramagnetic minerals contribute 14.94 per cent or more to total susceptibility (Table 1), paramagnetic behaviour dominates the thermomagnetic heating curves (Fig. 5a). Where paramagnetic minerals contribute over 37.99 per cent to the total susceptibility, paramagnetic behaviour completely suppresses all other indications (Table 1 and Fig 5a). Only where these contributions are much less significant, it is possible to identify any characteristics that may be indicative of other mineral phases without excluding the paramagnetic effect. Even where paramagnetic contributions to total susceptibility are minimal, for example, in the clay fractions from 0.51 Ma (3.77 per cent) and 6.96 Ma (4.98 per cent), there is no clear magnetite-type T_c and the gradual inflexion in the uncorrected heating curve occurs between 580 and 620 °C, with irreversible changes above 350 °C. However, once the paramagnetic component has been subtracted, there are strong indications of a T_c just above 600 °C. Such behavior may be indicative of fine-grained maghemite as the main ferrimagnetic phase in the clays (cf. Spassov *et al.* 2003).

A Verwey transition near 120 K, taken as evidence of magnetite, was not observed in the low-temperature susceptibility curves of fine fractions (<2 and 2–4 μm) from our selected 22 Ma samples (Oldfield *et al.* 2009), also supporting the view that maghemite is the dominant pedogenic ferrimagnet in most cases. These results are consistent with several previous investigations on Quaternary loess samples. The Verwey transition is very clear in bulk loess samples or coarse fractions that comprise detrital magnetite, but is greatly suppressed in the palaeosols samples (Banerjee *et al.* 1993; Eyre & Shaw 1994; Sartori *et al.* 1999, 2005; Liu *et al.* 2003, 2005), and disappears in the fine fractions (Sartori *et al.* 1999; Liu *et al.* 2003, 2005).

One of the more consistent features of those heating curves not dominated by paramagnetism is the slight downward inflexion between 150 and 200 °C noted above. Similar inflexions were also observed in clay fractions of Chinese loess samples over the same temperature range (Spassov *et al.* 2003). The partial heating/cooling experiments on the clay fractions of samples from two soil/loess couplets indicate that the inflexion is irreversible (Fig. 5b). This inflexion may be caused by transformation of a thermally unstable ferrimagnetic mineral to hematite. The comparison of B_{cr} and B_c between samples at room temperature and their 220 °C products indicates that this mineral has similar hysteresis properties to those of other ferrimagnets, magnetite and maghemite, in loess deposits.

For the magnetization at the end of the cooling sequence to fall below that at the beginning of the experiment would be consistent with some conversion of maghemite to hematite as noted by Spassov *et al.* (2003). Similar evidence for the importance of hematite comes from the wasp-waisted nature of several of the hysteresis loops especially in older samples with minimal ferrimagnetic contributions (Fig. 4).

Table 2. Comparison of magnetic properties of selected clay (<2 μm) and coarse (>8 μm) fractions and their thermal products in partial thermomagnetic experiment.

Particle fractions	Sample name	Age (Ma)	T (°C)	χ_{para} ($10^{-8}m^3\,kg^{-1}$)	M_{rs} ($10^{-3}Am^2\,kg^{-1}$)	M_s ($10^{-3}Am^2\,kg^{-1}$)	B_{cr} (mT)	B_c (mT)	M_{rs}/M_s	B_{cr}/B_c
<2 μm	QW-324	1.84	25	16.28	10.45	59.95	18.30	7.59	0.17	2.41
			220	15.59	10.38	56.43	17.74	7.13	0.18	2.49
	XF-331	1.87	25	15.93	7.13	41.00	18.28	7.07	0.17	2.59
			220	14.97	6.86	39.55	17.94	6.94	0.17	2.58
	QW-3481	21.73	25	13.80	3.27	11.36	58.03	16.39	0.29	3.54
			220	13.72	2.98	10.68	59.45	17.16	0.28	3.46
	QW-3497	21.83	25	13.41	2.56	8.70	124.15	21.77	0.29	5.70
			220	13.92	2.57	7.84	126.30	21.73	0.33	5.81
>8 μm	QW-324	1.84	25	5.08	7.89	41.58	44.09	14.45	0.19	3.05
			300	4.54	5.76	34.88	36.90	11.79	0.17	3.13
	XF-331	1.87	25	5.62	7.11	35.54	50.08	15.97	0.20	3.14
			300	5.31	5.14	31.22	42.57	13.71	0.16	3.10
	QW-3481	21.73	25	3.52	4.75	28.77	38.98	10.42	0.16	3.74
			300	3.05	3.92	24.26	37.73	10.20	0.16	3.70
	QW-3497	21.83	25	4.17	3.48	21.79	43.86	10.14	0.16	4.33
			300	3.75	3.07	19.98	41.28	9.99	0.15	4.13

Table 3. Viscous loss of IRM between 100 and 1000 s expressed as a percentage of the IRM at 100 s for six samples.

Age (Ma)	Sample	Lithology	Fractions	Viscous loss (per cent)				
				20 mT	40 mT	100 mT	300 mT	800 mT
0.51	97XF-1314	S5SS1	<2 μm	9.6	6.0	5.1	4.8	4.5
			>8 μm	2.6	–	–	–	2.0
1.84	97XF-324	S25	<2 μm	8.9	5.5	4.1	4.2	4.1
			>8 μm	2.1	–	–	–	1.5
2.62	97XFRC-61	Red Earth	<2 μm	8.8	5.3	4.6	4.4	4.2
			>8 μm	1.9	–	–	–	1.5
4.26	01DW-738	Loess	<2 μm	8.3	6.0	4.6	3.8	4.6
			>8 μm	2.6	–	–	–	2.4
6.96	01DW-1302	Soil	<2 μm	8.1	5.6	4.7	4.0	4.7
			>8 μm	2.9	–	–	–	2.4
15.44	99QW-1603	Soil	<2 μm	7.1	4.6	4.2	3.9	3.7
			>8 μm	1.2	–	–	–	1.5

5.2 Magnetic mineralogy of the coarse fractions

The clearest evidence for the presence of magnetite comes from the coarse fractions, especially from samples younger than ∼14 Ma. The SEM photomicrographs of iron oxides in the coarse fractions (Oldfield *et al.* 2009), the magnetic properties reported in that paper and in Hao *et al.* (2008b) and the minimal viscous loss of IRM in coarse fraction separates in low-reverse fields (Table 3) confirm that the magnetite recorded lacks a significant superparamagnetic contribution and is at least in part likely to be multidomain (MD). Evidence for an MD component is least clear in samples older than 15 Ma.

In most of the older samples, the inflexion at ∼300 °C (Fig. 5a) becomes more notable. From this, we infer that thermally unstable maghemite, related to low-temperature oxidation of magnetite, inverts to hematite (*cf*. Spassov *et al.* 2003). The partial heating experiments indicate that transformation to hematite started around 300–350 °C (Fig. 5b). Low-temperature oxidation of magnetite to maghemite under natural conditions is common for loess deposits (van Velzen & Dekkers 1999). The stress between magnetite core and maghemite rim leads to an increase in coercivity which can be reversed by heating up to 150 °C (van Velzen & Dekkers 1999). The stepwise heating experiments confirm that heating up to 150 °C can remove most of the influence of partial oxidation on the hysteretic properties, and further heating up to 300 °C only leads to a decrease in hysteretic properties with a much reduced amplitude (Liu *et al.* 2004). The decrease in the hysteresis properties (M_{rs}, M_s, B_{cr} and B_c) after heating up to 300 °C for the coarse fraction of four samples (Table 2) is consistent with the partial oxidation model of magnetite (van Velzen & Dekkers 1999; Liu *et al.* 2004). From the above, we infer that partial oxidation of magnetite to maghemite in the coarse fractions has occurred especially in the older samples.

The consistent tendency for magnetization corrected for paramagnetism to fall below the zero line at high temperatures in the coarse fractions we ascribe to a significant diamagnetic effect of the high quartz content in these fractions. Hysteresis measurements as a function of temperature show that the changes in magnetization of quartz-rich loess samples above ∼0.3 T are dominated by diamagnetic components at high temperatures, with a much less significant diamagnetic effect in palaeosol sample (Sartori *et al.* 2005).

5.3 Hysteresis loops, Day plots and ferrimagnetic grain size

Fig. 6 shows the Day plot (Day *et al.* 1977; Dunlop 2002a,b) derived from the hysteresis data, plotted with envelopes of values from earlier studies. Data from both the coarse and most of the clay

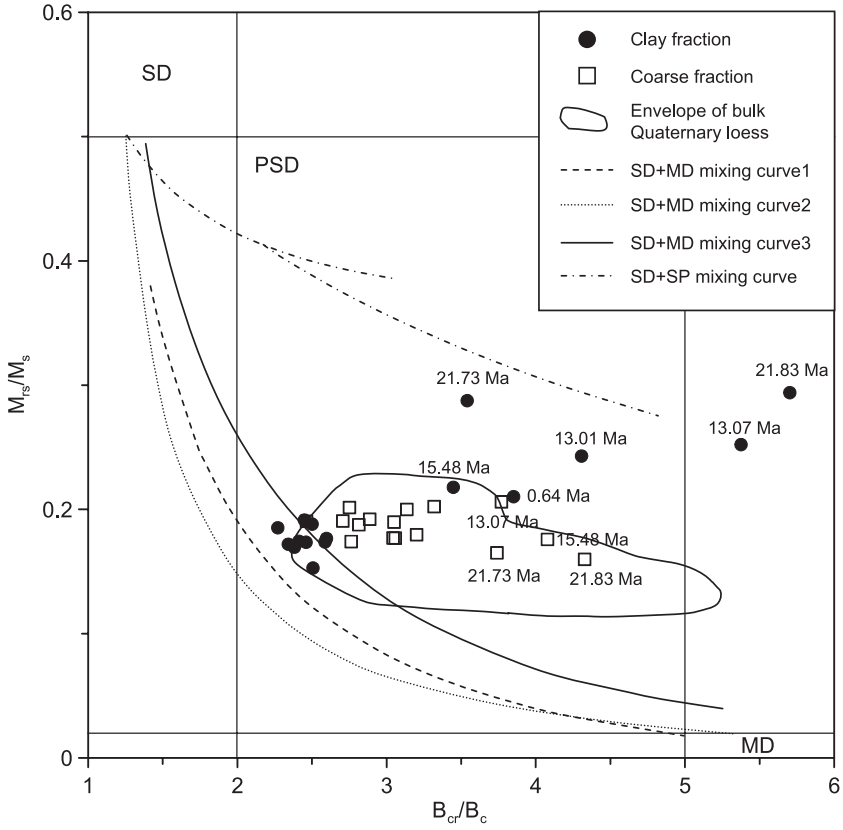

Figure 6. Day Plot (Day *et al.* 1977), along with the Dunlop mixing curves (Dunlop 2002a,b), of the hysteresis data for all the clay (<2 μm) and coarse (>8 μm) fractions over the last 22 Myr, plotted with envelopes of values from earlier studies on Pleistocene bulk loess and soil samples (Liu *et al.* 1992, 2003; Fukuma & Torii 1998; Deng *et al.* 2004; Wang *et al.* 2006).

fractions plot within a rather restricted zone showing relatively little variation in M_{rs}/M_s and a twofold variation in B_{cr}/B_c. Only two samples, clay fractions from 13.07 and 21.83 Ma have distinctively high values for B_{cr}/B_c. The clay fractions with S-ratio values $\leq$0.78 (Table 1) lie above all others that have S ratios $\geq$0.92.

The parameters shown in the Day plot (Fig. 6) place all the coarse fractions within the envelope of values given for loess and palaeosol samples in previous studies (Liu *et al.* 1992, 2003; Fukuma & Torii 1998; Deng *et al.* 2004; Wang *et al.* 2006). The tightly grouped majority of the clay samples have lower B_{cr}/B_c values than do the coarse fractions and lie close to or on the edge of the same envelope, within or close to the range of synthetic MD + SD mixing curves in Dunlop (2002b). This ascription is contradicted by the many susceptibility and remanence measurements outlined in our previous publications, especially the MPMS-derived low-temperature results summarized in Oldfield *et al.* (2009). Table 3 also confirms the presence of fine viscous grains in such samples. All point to the dominance of these samples by a mixture of SP, SD and fine viscous grains. We conclude that here, fine viscous, as distinct from true SD or SP grains, are difficult to distinguish from MD grains, as is also the case in routine DC demagnetization of SIRM experiments. Four clay samples from the periods of lowest magnetic concentrations in the early and mid-Miocene form outliers with higher M_{rs}/M_s values than all the others. These lie close to Dunlop's (2002b) SD+SP mixing lines as would be predicted from their other magnetic properties. Only two samples lie between the two groups discussed above. Although the Day plot distinguishes between the clay and coarse fractions, it does not do so in a way that is either consistent or compatible with other lines of evidence. Further numerical magnetic modelling of hysteresis loops is needed to get a better understanding of these rather complex natural mixtures (e.g. Tauxe *et al.* 1996, 2002; Dunlop & Ödemir 1997).

5.4 The effects of hematite on the apparent paramagnetic susceptibility

In most of the foregoing discussion, the possible contribution of hematite to the 'paramagnetic' susceptibility inferred from the hysteresis data has been ignored. Irrespective of any possible hematite contribution, the strong influence and, at times dominance of true paramagnetic contributions can be confirmed not only from the data presented here, but also from the low-temperature experiments conducted using the magnetic properties measuring system (MPMS) and reported in Oldfield *et al.* (2009). Nevertheless, there are indications that a possible contribution of hematite to 'paramagnetic' susceptibility cannot be excluded. $\mathrm{Hard}_{100\mathrm{mT}}$ (the part of the SIRM that remains un-reversed after application of a field of −100 mT) provides a basis for estimating the contribution from high-coecivity magnetic components to SIRM values, here mainly related to hematite. The crossplots of χ_{para} versus $\mathrm{Hard}_{100\mathrm{mT}}$ of the clay and coarse fractions are shown in Fig. 7. There is a significant positive correlation between χ_{para} and $\mathrm{Hard}_{100\mathrm{mT}}$ for the clay fractions above the two bottom samples, but a much weaker correlation for the coarse fractions. The difference in the slopes of the linear fit lines between the clay and coarse fractions is remarkable. As the

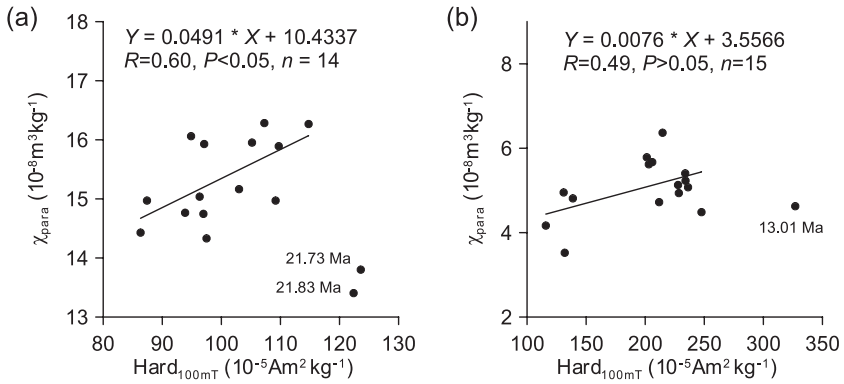

Figure 7. Crossplots of paramagnetic susceptibility and $Hard_{100mT}$ for all the clay (<2 μm; a) and coarse (>8 μm; b) fractions over the last 22 Myr. The linear fit in (a) is based on the samples above the two oldest samples and in (b), on samples except sample ZW-578 (13.01 Ma).

pedogenic processes in loess deposits generate both paramagnetic minerals (e.g. Deng *et al.* 2004) and hematite (e.g. Torrent *et al.* 2006), the higher slope for the clay fractions is at least partly related to pedogentic processes. We use the high-field susceptibility of hematite $\chi_{hm} = 97 \times 10^{-8}$ m^3 kg^{-1} (Peters & Dekkers 2003) and the hematite content (Table 1) to estimate a maximum hematite contribution. The maxima hematite content is 27.11 g kg^{-1} (Table 1), representing a maximum contribution to susceptibility of 2.63×10^{-8} m^3 kg^{-1} for the clay fractions, almost an order of magnitude less than the total paramagnetic susceptibility. This implies that despite the correlation noted, the hematite effect on the χ_{para} calculation in the clay fraction is rather weak.

5.5 Clay fractions in palaeosols and loess

Paramagnetic susceptibility varies little between palaeosols and loess layers within the same couplet, which tends to amplify the contrast between the two in χ_{ferri} values. Also, as a consequence, χ_{para}/χ and χ_{para}/M_s are higher in the loess layers. The reduced influence of fine-grained, low-coercivity ferrimagnets in the loess layers also leads to generally higher values of B_c and B_{cr}. Thus, all the main differences noted in the present data set between the clay fractions in the loess and palaeosol layers are largely controlled by the effects of pedogenesis in the latter.

5.6 Coarse fractions in palaeosols and loess

The χ_{para}/χ and χ_{para}/M_s values are higher in loess than in palaeosols in each loess–palaeosol pair, as, in most cases, are values for χ_{para} and B_{cr}. Even in the coarse fractions, χ_{ferri} values are higher in palaeosol than in loess layers. This may reflect, in part, some contamination of the coarse fraction, though previous results (Hao *et al.* 2008b; Oldfield *et al.* 2009) suggest that this is negligible. It is therefore possible that there is a real difference in the balance between non-magnetic (e.g. silicates) and magnetic minerals in the loess–palaeosol pairs. This, in turn, may indicate a difference in source materials or transport effectiveness. Many more particle size-based measurements would be required to confirm or otherwise.

5.7 Distinctions between clay and coarse fractions

The main distinctions between the clay and coarse fractions, reflecting higher concentrations of fine-grained ferrimagnetic minerals in the former, have already been noted elsewhere (Hao *et al.* 2008b; Oldfield *et al.* 2009). This study adds two additional contrasts. The clay fractions contain consistently higher concentrations of paramagnetic minerals. Although those present in the coarse fraction are likely to represent detrital rock fragments of, for example, iron-bearing silicates, those in the clays are likely to represent weathering products such as illite (Bronger & Heinkele 1990; Gylesjö & Arnold 2006). There is also an apparent contrast in the degree of oxidation of the ferrimagnetic minerals present. In the post-Miocene samples, the detrital ferrimagnets show a magnetite-type T_c, whereas the dominant ferrimagnetic mineral in all the clay fractions is more likely to be maghemite. Whether this contrast reflects a distinction between the mineralogy of the original detrital and pedogenic minerals or is mainly a function of the interaction between magnetic grain size and post-depositional diagenesis is considered below.

5.8 Changes through time

There is no strong trend in χ_{para} values in the clays, though values are mainly higher in fractions from samples postdating 7 Ma. Apart from this, virtually all the long-term changes detectable in the VFTB data are expressing the degree to which other properties are controlled by variations in the contributions from ferrimagnetic minerals and especially those resulting from pedogenesis in the palaeosols. One clear measure of this comes from comparing the χ_{ferri} for the Pleistocene samples with those from the two Miocene age samples representing the two long periods of minimum susceptibility between 8.5 and 22 Ma. In the case of the clay fractions from the palaeosols, the ratio is 26.4:1 and in the clays from the loess layers, 2.3:1. In the case of the coarse fractions, the ratios in both the palaeosols and the loess layers are 2.3:1 and 1.1:1, respectively. The main long-term changes therefore reflect major differences in the final products of soil formation.

From the magnetic measurements alone, there remain three possible interpretations. Adopting the model expounded by Torrent *et al.* (2006), the Miocene palaeosols with minimum χ_{ferri} values in the clay fractions would be seen as the ones in which pedogenic transformation of ferrihydrite in the soil layers was most complete. These then, would be the most maturely weathered palaeosols. None of the evidence derived from the VFTB measurements would contradict this interpretation, though it is worth noting that, from the DRS results and high-field remanence measurements, hematite is not actually more abundant in these Miocene palaeosols than in younger ones (Hao *et al.* 2009). Moreover, they are not marked by

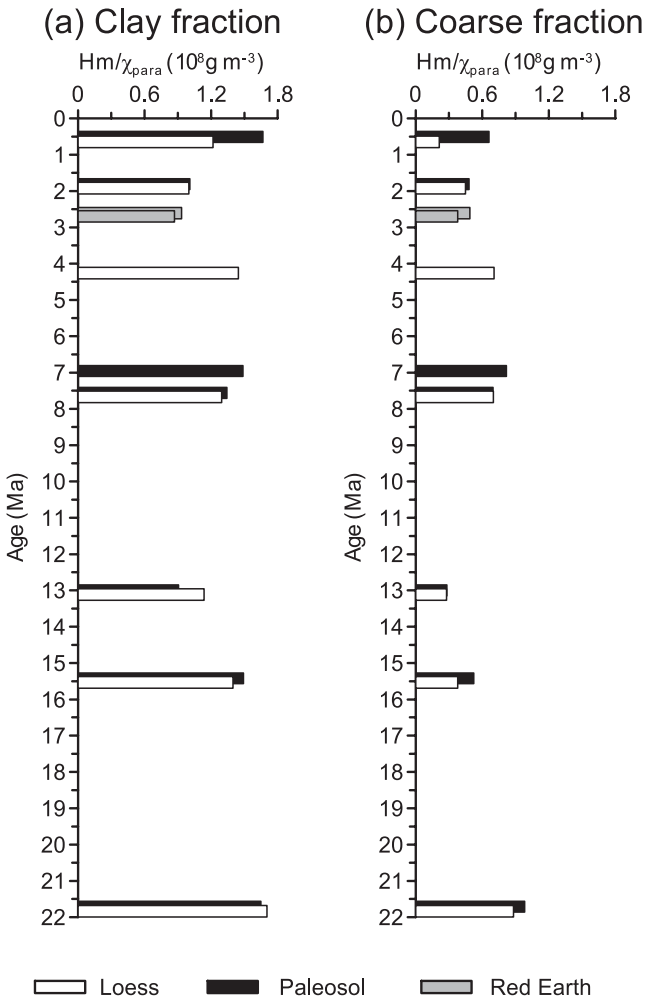

Figure 8. Quotient of hematite content derived from the DRS measurements (Hao *et al.* 2009), over paramagnetic susceptibility (Hm/χ_{para}) against age for all the clay (<2 μm; a) and coarse (>8 μm; b) fractions over the last 22 Myr.

any higher values in the ratio of hematite to χ_{para} (Fig. 8) save in the case of the two basal samples. Adopting the Maher & Thompson (1992, 1999) interpretation, the Miocene samples with minimum χ_{ferri} in the clay fractions would be seen as indicative of a significantly drier weathering regime leading to a different enhancement pathway. As originally proposed, this interpretation would lead us to expect to see clear evidence from the thermomagnetic experiments for magnetite as the main carrier, but this is not the case. The third possibility would invoke the influence of long-term diagenesis impacting the magnetic mineralogy of the iron oxides on timescales well beyond the orbital time frames controlling palaeosol/loess alternations. This could involve some form of oxidative diagenesis, akin perhaps to the maghematization recorded in marine red bed sediments (e.g. Kent & Lowrie 1974; Johnson *et al.* 1975; van Velzen & Zijderveld 1992, 1995; van Velzen & Dekkers 1999) and the process would be strongly sensitive to contrasts in grain size (van Velzen & Dekkers 1999). Indications from the thermomagnetic experiments that the finest fractions are probably maghemite-dominated in all samples, but that only the coarse fractions in the oldest samples, postdating 15 Ma, lack a clear magnetite-type T_c, would support this interpretation. This speculation opens up the possibility that the magnetic properties of the Miocene part of the record, notably those in the intervals with minimum χ_{ferri} values, are strongly affected by long-term post-depositional diagenesis, though the high χ and χ_{ferri} values from 14.4 to 15.9 Ma run counter to this suggestion.

6 CONCLUSIONS

(1) The hysteresis plots and thermomagnetic experiments on all the samples considered here reinforce previous indications from low-temperature experiment on five samples from the Dongwan and QA–I parts of the sequence (Oldfield *et al.* 2009) that paramagnetic minerals make a major contribution to the clay fractions throughout the whole period studied.

(2) The only samples in which magnetite clearly dominates the thermomagnetic properties are the post-Miocene coarse fractions.

(3) The degree of oxidation indicated by the thermomagnetic curves is highest in the clays and next highest in the oldest coarse fractions suggesting that both grain size and sample age have affected this process.

(4) Our data show a clear contrast in thermomagnetic properties between the detrital and clay fractions, suggesting that inferences based on thermomagnetic experiments on bulk samples may fail to take into account the complex nature of magnetic mineralogy, especially in soil samples where both pedogenic and detrital minerals are present.

(5) Day plots appear to misdiagnose the grain size composition of samples with a significant contribution from fine viscous grains. Consequently, they provide limited and potentially misleading information on the differences between fine-grained pedogenic and coarse-grained detrital ferrimagnetic assemblages, even when allowance is made for the possible effects of hematite on the quotients used.

(6) Separation of the ferrimagnetic and paramagnetic contributions to total susceptibility highlight the extent to which the contrasts between loess and palaeosol layers, as well as the changes in the clay fractions linked to age are driven by differences in the concentration of fine grained, pedogenic ferrimagnetic minerals.

(7) The extent to which the low-ferrimagnetic concentrations typical of the clay fractions in most of the Miocene part of the record reflect drier climatic conditions during formation, more complete pedogenesis or oxidative diagenesis on supra-orbital timescales still remains unresolved by magnetic measurements alone.

ACKNOWLEDGMENTS

This study was supported by the National Basic Research Program of China (973 Program; No: 2010CB950204), the National Natural Science Foundation of China (No: 41172323), Ministry of Land and Resources (No: 201211077) and J. Bloemendal and Q. Hao thank the Royal Society for financial support. We thank Drs M. Brown and M. Hill for helps in VFTB measurement, R. Jude for help with the magnetic measurements and A. Henderson, I. Cooper and H. Hull for help in particle separation. Q. Hao also thanks Dr. C. Deng for helps in the experiments and calculations.

REFERENCES

Banerjee, S.K., Hunt, C.P. & Liu, X.-M., 1993. Separation of local signals from the regional paleomonsoon record of the Chinese loess plateau: a rock-magnetic approach, *Geophys. Res. Lett.,* **20,** 843–846.

Bloemendal, J., King, J.W., Hall, F.R. & Doh, S.-J., 1992. Rock magnetism of late Neogene and Pleistocene deep-sea sediments: relationship to sediment source, diagenetic processes, and sediment lithology, *J. geophys. Res.,* **97**(B4), 4361–4375, doi:10.1029/91JB03068.

Bronger, A. & Heinkele, T., 1990. Mineralogical and clay mineralogical aspects of loess research, *Quat. Int.,* **7/8,** 37–52.

Chen, F., Wu, R., Pompei, D. & Oldfield, F., 1995. Magnetic property and particle size variations in the late Pleistocene and Holocene parts of the Dadongling loess section near Xining, China, *Quat. Proc.,* (4), 27–40.

Day, R., Fuller, M. & Schmidt, V.A., 1977. Hysteresis properties of titanomagnetites: grain-size and compositional dependence, *Phys. Earth planet. Inter.,* **13,** 260–267.

Deng, C., Zhu, R., Verosub, K.L., Singer, M.J. & Vidic, N.J., 2004. Mineral magnetic properties of loess/paleosol couplets of the central loess platesu of China over the last 1.2 Myr, *J. geophys. Res.,* **109**(B01103), doi:10.1029/2003JB002532.

Deng, C.L., Vidic, N.J., Verosub, K.L., Singer, M.J., Liu, Q.S., Shaw, J. & Zhu, R.X., 2005. Mineral magnetic variation of the Jiaodao Chinese loess/paleosol sequence and its bearing on long-term climatic variability, *J. geophys. Res.,* **110**(B03103), doi:10.1029/2004JB003451.

Dunlop, D.J., 2002a. Theory and application of the Day plot (Mrs/Ms versus Hcr/Hc). 1. Theoretical curves and tests using titanomagnetite data, *J. geophys. Res.,* **107**(B3), doi:10.1029/2001JB000487.

Dunlop, D.J., 2002b. Theory and application of the Day plot (Mrs/Ms versus Hcr/Hc). 2. Application to data for rocks, sediments, and soils, *J. geophys. Res.,* **107**(B3), doi:10.1029/2001JB000486.

Dunlop, D.J. & Ödemir, Ö., 1997. *Rock Magnetism: Fundamentals and Frontiers,* pp. 316–323, Cambridge University Press, Cambridge.

Evans, M.E. & Heller, F., 2001. Magnetism of loess/palaeosol aequence:recent developments, *Earth-Sci. Rev.,* **54,** 129–144.

Eyre, J.K. & Shaw, J., 1994. Magnetic enhancement of Chinese loess-the role of Fe_2O_3, *Geophys. J. Int.,* **117,** 265–271.

Fukuma, K. & Torii, M., 1998. Variable shape of magnetic hysteresis loops in the Chinese loess-paleosol sequence, *Earth, PlanetsSpace,* **50**(1), 9–14.

Guo, Z. *et al*., 1998. Climate extremes in Loess of China coupled with the strength of deep-water formation in the North Atlantic, *Global planet. Change,* **18,** 113–128.

Guo, Z.T., Peng, S.Z., Hao, Q.Z., Biscaye, P.E. & Liu, T.S., 2001. Origin of the Miocene-Pliocene red-earth formation at Xifeng in Northern China and implications for paleoenvironments, *Palaeogeog., Plaeoclimat., Palaeoecol.,* **170,** 11–26.

Guo, Z.T. *et al*., 2002. Onset of Asian desertification by 22 Myr ago inferred from loess deposits in China, *Nature,* **416,** 159–163.

Gylesjö, S. & Arnold, E., 2006. Clay mineralogy of a red clay-loess sequence from Lingtai, the Chinese Loess Plateau, *Global planet.Change,* **51**(3–4), 181–194.

Hao, Q. & Guo, Z., 2004. Magnetostratigraphy of a late Miocene-Pliocene loess-soil sequence in the western Loess Plateau in China, *Geophs. Res. Lett.,* **31,** L09209, doi:10.1029/2003GL019392.

Hao, Q. & Guo, Z., 2005. Spatial variations of magnetic susceptibility of Chinese loess for the last 600 kyr: implications for monsoon evolution, *J. geophys. Res.,* **110,** B12101, doi:10.1029/2005JB003765.

Hao, Q.Z., Oldfield, F., Bloemendal, J. & Guo, Z.T., 2008a. The magnetic properties of loess and paleosol samples from the Chinese Loess Plateau spanning the last 22 million years, *Palaeogeog. Palaeoclimat. Palaeoecol.,* **260**(3–4), 389–404.

Hao, Q.Z., Oldfield, F., Bloemendal, J. & Guo, Z.T., 2008b. Particle size separation and evidence for pedogenesis in samples from the Chinese Loess Plateau spanning the past 22 m.y., *Geology,* **36**(9), 727–730.

Hao, Q., Oldfield, F., Bloemendal, J., Torrent, J. & Guo, Z., 2009. The record of changing Hematite and Goethite deposition over the last 22 Ma on the Chinese Loess Plateau from magnetic measurements and Diffuse Reflectance Spectroscopy, *J. geophys. Res.,* **114,** B12101, doi:10.1029/2009JB006604.

Heller, F. & Evans, M.E., 1995. Loess magnetism, *Rev. Geophys.,* **33**(2), 211–240.

Johnson, H.P., Kinoshita, H. & Merrill, R.T., 1975. Rock magnetism and paleomagnetism of some North Pacific deep-sea sediments, *Geol. Soc. Am. Bull.,* **86,** 412–420.

Kent, D.V. & Lowrie, W., 1974. Origin of magnetic instability in sediment cores from the central North Pacific, *J. geophys. Res.,* **79,** 2987–3000.

Liang, M., Guo, Z., Kahmann, A.J. & Oldfield, F., 2009. Geochemical characteristics of the Miocene eolian deposits in China: their provenance and climate implications, *Geochem. Geophys. Geosys.,* **10**(4), Q04004, doi:10.1029/2008GC002331.

Liu, X., Shaw, J., Liu, T., Heller, F. & Yuan, B., 1992. Magnetic mineralogy of Chinese loess and its significance, *Geophys. J. Int.,* **108,** 301–308.

Liu, X.-M., Bloemendal, J., Rolph, T., Shaw, J., Liu, T.-S. & Heller, F., 1995. Quantitative estimates of palaeoprecipitation at Xifeng in the loess plateau of China, *Palaeogeog., Palaeoclimat., Palaeoecol.,* **113,** 243–248.

Liu, Q., Banerjee, S.K., Jackson, M.J., Chen, F., Pan, Y. & Zhu, R., 2003. An integrated study of the grain-size-dependent magnetic mineralogy of the Chinese loess/paleosol and its environmental significance, *J. geophys. Res.,* **108**(B9), 2437, doi:10.1029/2002JB002264.

Liu, Q.S., Banerjee, S.K., Jackson, M.J., Deng, C.L., Pan, Y.X. & Zhu, R.X., 2004. New insights into partial oxidation model of magnetites and thermal alteration of magnetic mineralogy of the Chinese loess in air, *Geophys. J. Int.,* **158,** 506, 514.

Liu, Q.S., Torrent, J., Maher, B.A., Yu, Y.J., Deng, C.L., Zhu, R.X. & Zhao, X.X., 2005. Quantifying grain size distribution of pedogenic magnetic particles in Chinese loess and its significance for pedogenesis, *J. geophys. Res.,* **110**(B11102), doi:10.1029/2005JB003726.

Maher, B.A. & Thompson, R., 1992. Paleoclimatic significance of the mineral magnetic record the Chinese loess and paleosols, *Quat. Res.,* **37,** 155–170.

Maher, B.A. & Thompson, R., 1999. Palaeomonsoons 1: the magnetic record of palaeoclimate in the terrestrial loess and palaeosol sequences, in *Quaternary Climates, Environments and Magnetism,* pp. 81–125, eds Maher, B.A. & Thompson, R., Cambridge University Press, Cambridge.

Oldfield, F., Hao, Q., Bloemendal, J., Gibbs-Eggar, Z., Patil, S. & Guo, Z., 2009. Links between particle size and magnetic grain size: general observations and some implications for Chinese loess studies, *Sedimentology,* **56,** 2091–2106, doi: 10.1111/j.1365-3091.2009.01071.x.

Peters, C. & Dekkers, M.J., 2003. Selected room temperature magnetic parameters as a functionof mineralogy, concentration and grain size, *Phys. Chem. Earth,* **28,** 659–667.

Qiao, Y.S., Guo, Z.T, Hao, Q.Z., Yin, Q.Z., Yuan, B.Y. & Liu, T.S., 2006. Grain–size features of a Miocene loess–soil sequence at Qinan: inplications on its origin, *Sci. China, Ser. D: Earth Sci.,* **49,** 731–738.

Sartori, M., Heller, F., Forster, T., Borkovec, M., Hammann, J. & Vincent, E., 1999. Magnetic properties of loess grain size fractions from the section at Paks (Hungary), *Phys. Earth planet. Inter.,* **116**(1), 53–64.

Sartori, M., Evans, M.E., Heller, F., Tsatskin, A. & Han, J.M., 2005. The last glacial/interglacial cycle at two sites in the Chinese Loess Plateau: mineral magnetic, grain-size and ^{10}Be measurements and estimates of palaeoprecipitation, *Palaeogeog. Palaeoclimat. Palaeoecol.,* **222**(1–2), 145–160.

Spassov, S., Heller, F., Kretzschmar, R., Evans, M.E., Yue, L.P. & Nourgaliev, D.K., 2003. Detrital and pedogenic magnetic mineral phases in the loess/palaeosol sequence at Lingtai (Central Chinese Loess Plateau), *Phys. Earth planet. Inter.,* **140,** 255–275.

Sun, D., An, Z., Shaw, J., Bloemendal, J. & Sun, Y., 1998. Magnetostratigraphy and palaeoclimatic significance of Late Tertiary aeolian sequences in the Chinese Loess Plateau, *Geophys. J. Int.,* **134**(1), 207–212.

Tauxe, L., Mullender, T.A.T. & Pick, T., 1996. Potbellies, wasp-waists, and superparamagnetism in magnetic hysteresis, *J. geophys. Res.,* **101,** 571–583.

Tauxe, L., Bertram, H.N. & Seberino, C., 2002. Physical interpretation of hysteresis loops: micromagnetic modeling of fine particle magnetite, *Geochem. Geophys. Geosyst.,* **3**(10), 1–22.

Torrent, J., Barron, V. & Liu, Q.S., 2006. Magnetic enhancement is linked to and precedes hematite formation in aerobic soil, *Geophys. Res. Lett.,* **33,** L02401, doi:10.1029/2005GL024818.

van Velzen, A.J. & Dekkers, M.J., 1999. Low-temperature oxidation of magnetite in loess-paleosol sequences: a correction of rock magnetic parameters, *Stud. geophys. geod.,* **43**(4), 357–375.

van Velzen, A.J. & Zijderveld, J.D.A., 1992. A method to study alterations of magnetic minerals during thermal demagnetization applied to a fine-grained marine marl (Trubi formation, Sicily), *Geophys. J. Int.,* **110,** 79–90.

van Velzen, A.J. & Zijderveld, J.D.A., 1995. Effects of weathering on single-domain magnetite in Early Pliocene marine marls, *Geophys. J. Int.,* **121,** 267–278.

Wang, X.Y., Lu, H.Y., Xu, H.F., Deng, C.L. & Chen, T.H., 2006. Magnetic properties of loess deposits on the northeastern Qinghai-Tibetan Plateau: palaeoclimatic implications for the Late Pleistocene, *Geophys. J. Int.,* **167**(3), 1138–1147.

Zheng, H.-B., Oldfield, F., Yu, L., Shaw, J. & An, Z.-S., 1991. The magnetic properties of particle-sized samples from the Luochuan loess section: evidence for pedogenesis, *Phys. Earth planet. Inter.,* **68,** 250–258.